Supporting Information

Table S1. The impurities for *Ln*CrAsO (*Ln* = La, Ce, Pr, and Nd) samples

Ln	La	Ce	Pr	Nd
*Ln*CrAsO (mol%)	91.7(2)	89.3(3)	84.9(2)	84.1(3)
Ln_2O_3 (mol%)	1.4(7)	1.9(7)	13.8(8)	8.3(5)
CrAs (mol%)	7.9(4)	8.8(4)	1.3(7)	7.6(4)
Total (mol%)	100.0	100.0	100.0	100.0

Table S2. Fitting parameters for the Curie-Weiss formula with a temperature-independent term (χ_0) for *Ln*CrAsO.

Ln	Ce	Pr	Nd
χ_0 (emu/mol)	1.49×10^{-3}	1.60×10^{-3}	8.45×10^{-4}
θ (K)	-17.3	-11.3	-16.9
C (K cm^3/mol)	0.634	1.29	1.52
μ (μ_B/*Ln*)	2.25	3.21	3.49
Temp. range (K)	38-300	38-300	16-300

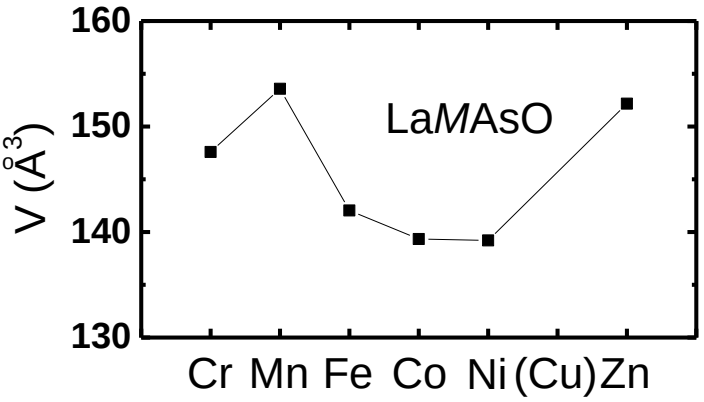

Figure S1. Variation of cell volume for 1111-type La*M*AsO (*M* = 3*d* transition metal ion) at RT.[1–5]

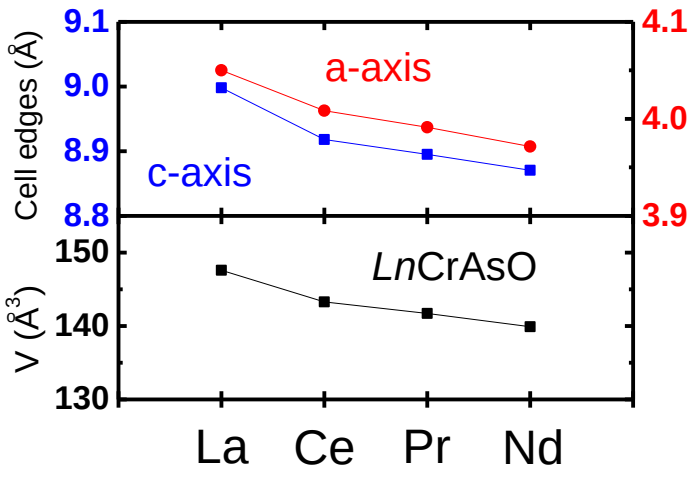

Figure S2. Variation of cell edges and volumes for *Ln*CrAsO (*Ln* = La, Ce, Pr, and Nd) at RT. From La to Nd, diffraction peaks shift to higher angles, indicating that the unit cell shrinks because of lanthanide contraction.

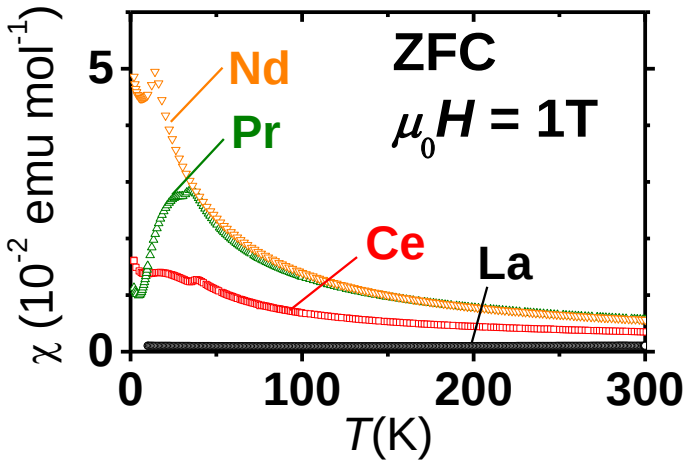

Figure S3. Temperature dependence of magnetic susceptibility (χ) for *Ln*CrAsO (*Ln* = La, Ce, Pr, and Nd) under 1 T.

For LaCrAsO, temperature-independent magnetic susceptibility (Pauli PM) was observed over the whole temperature range. For *Ln* = Ce, Pr and Nd, the magnetic susceptibility increased with decreasing temperature (Curie-Weiss behavior), and it shows a cusp related to the AFM transition because of the ordering of the *Ln* $4f^n$ spin below 40 K. Neel temperature T_N for these *Ln* $4f^n$ spin were 38.5 K, 38.0 K, and 14.2 K for *Ln* = Ce, Pr, and Nd, respectively. The magnetic parameters obtained from the modified Curie-Weiss equation, $\chi = C / (T - \theta) + \chi_0$, where C, θ and χ_0 are Curie constant, Weiss constant, and the temperature-independent term, respectively, are summarized in Table S2. The effective Bohr magneton values for *Ln*CrAsO (*Ln* = Ce, Pr, and Nd) were 2.25, 3.21, and 3.49 μ_B, respectively. These values agree well with the theoretical effective Bohr magneton values of 2.54, 3.58, and 3.62 μ_B for Ce^{3+}, Pr^{3+}, and Nd^{3+}, respectively, indicating that the *Ln* ions are in a trivalent state.

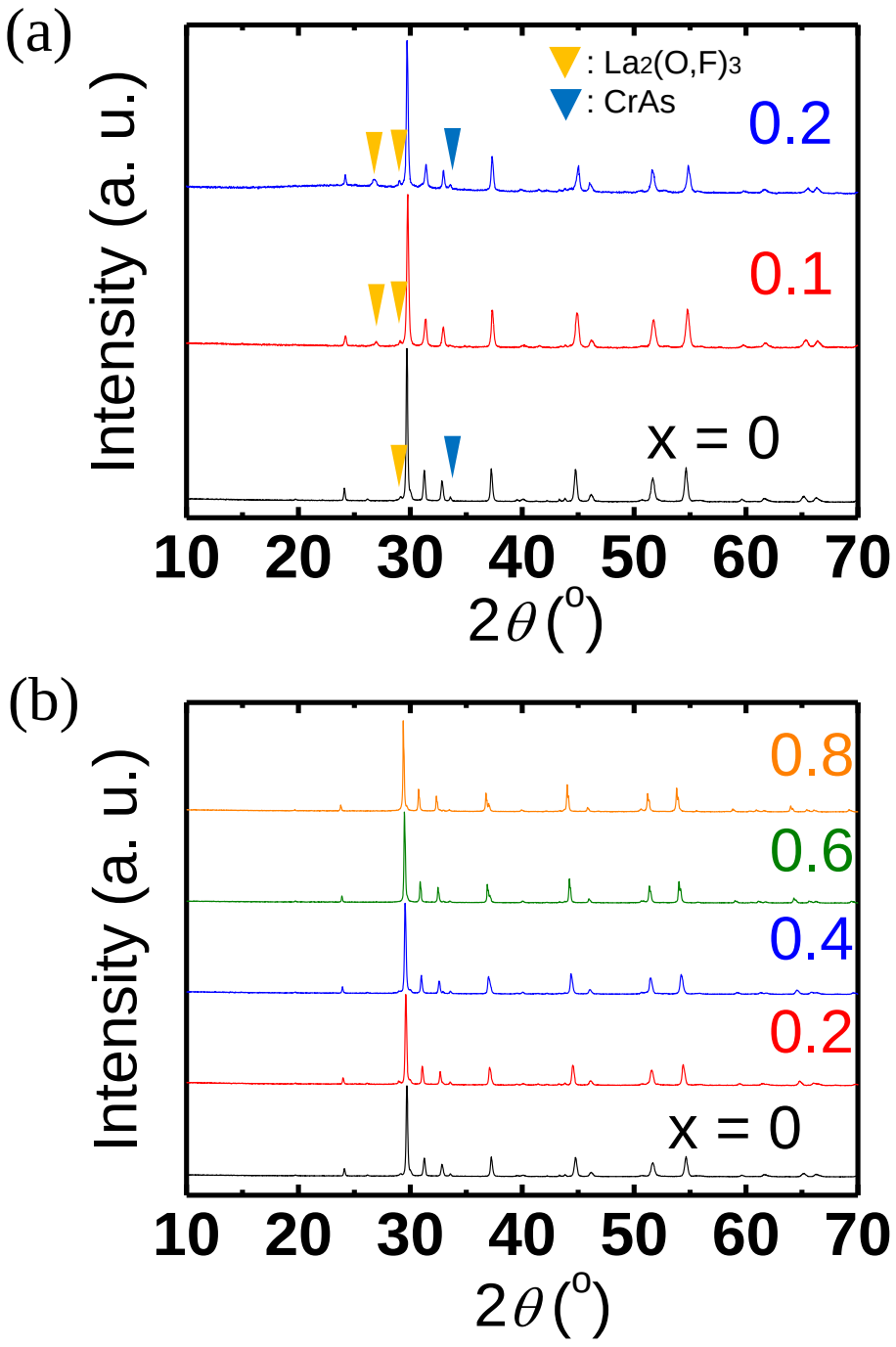

Figure S4. Powder XRD patterns of $LaCrAs(O_{1-x}F_x)$ (a) and $La(Cr_{1-x}Mn_x)AsO$ (b).

For F-doped LaCrAsO samples, the diffraction peaks derived from impurities including CrAs and $La_2(O,F)_3$ appeared as the amount of dopant is increased. On the other hand, no impurity peak for Mn-doped LaCrAsO samples was observed, except for that of only a small amount of (Cr,Mn)As.

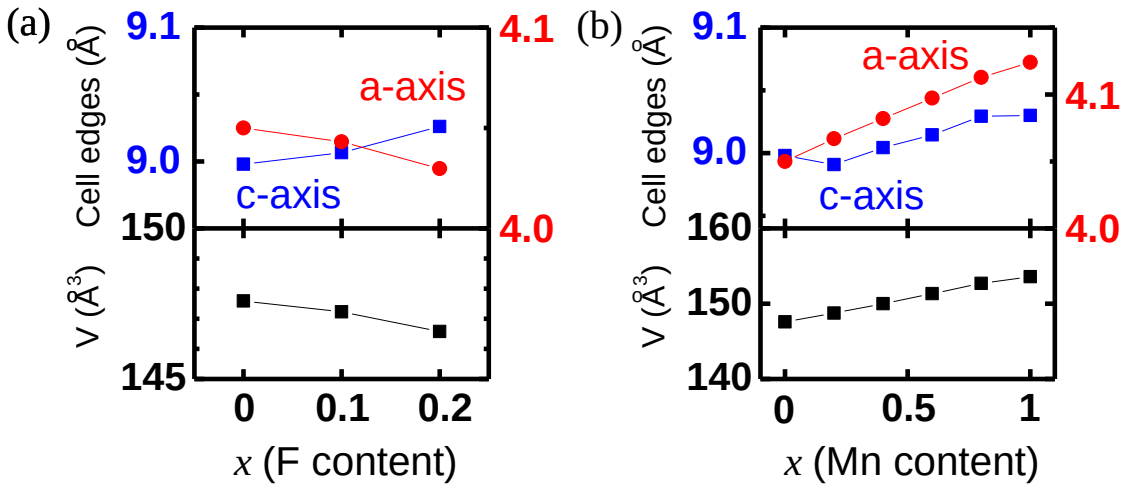

Figure S5. Variation of cell edges and volumes for (a) $LaCrAs(O_{1-x}F_x)$, and (b) $La(Cr_{1-x}Mn_x)AsO$.

The cell edges of $LaCrAs(O_{1-x}F_x)$ varied with x, and a monotonic decrease in the unit cell volumes was observed. This fact seems reasonable because smaller-sized F^- ions are substituted for larger-sized O^{2-} ion sites.[6]

For $La(Cr_{1-x}Mn_x)AsO$, the cell volume increased with increasing x, suggesting that the smaller-sized Cr ion sites were substituted by larger-sized Mn ions for the full range of Mn content from 0 to 1.[6]

REFERENCES

(1) T. Nientiedt, ;W. Jeitschko, P. G.; Pollmeier; M. Brylak, Z.; Naturforsch., B. *Chem. Sci.* **1997**, *52*, 560.

(2) Sefat, A. S.; Huq, A.; McGuire, M. A.; Jin, R.; Sales, B. C.; Mandrus, D.; Cranswick, L. M. D.; Stephens, P. W.; Stone, K. H. *Phys. Rev. B* **2008**, *78*, 104505.

(3) Yanagi, H.; Kawamura, R.; Kamiya, T.; Kamihara, Y.; Hirano, M.; Nakamura, T.; Osawa, H.; Hosono, H. *Phys. Rev. B* **2008**, *77*, 224431.

(4) Watanabe, T.; Yanagi, H.; Kamihara, Y.; Kamiya, T.; Hirano, M.; Hosono, H. *J. Solid State Chem.* **2008**, *181*, 2117.

(5) Takano, Y.; Komatsuzaki, S.; Komasaki, H.; Watanabe, T.; Takahashi, Y.; Takase, K. *J. Alloy Compd.* **2008**, *451*, 467.

(6) Shannon, R. D. *Acta Crystallogr., Sect B* **1970**, *26*, 447.